Multiple Bragg diffraction in opal-based photonic crystals: Spectral and spatial dispersion

I. I. Shishkin,[1,2] M. V. Rybin,[1,2,*] K. B. Samusev,[1,2] V. G. Golubev,[1] and M. F. Limonov[1,2]

[1]*Ioffe Physical-Technical Institute of the Russian Academy of Sciences, St. Petersburg 194021, Russia*

[2]*National Research University for Information Technology, Mechanics and Optics (ITMO), St. Petersburg 197101, Russia*

(Received 24 September 2013; revised manuscript received 30 December 2013; published 16 January 2014)

We present an experimental and theoretical study of multiple Bragg diffraction from synthetic opals. An original setup permits us to overcome the problem of the total internal light reflection in an opal film and to investigate the diffraction from both the (111) and ($\bar{1}$11) systems of planes responsible for the effect. As a result, angle- and frequency-resolved diffraction and transmission measurements create a picture of multiple Bragg diffraction that includes general agreement between dips in the transmission spectra and diffraction peaks for each incident white light angle and a twin-peak structure at frequencies of the photonic stop band edges. Two opposite cases of the interference are discussed: an interference of two narrow Bragg bands that leads to multiple Bragg diffraction with anticrossing regime for dispersion photonic branches and an interference of a narrow Bragg band and broad disorder-induced Mie background that results in a Fano resonance. A good quantitative agreement between the experimental data and calculated photonic band structure has been obtained.

DOI: 10.1103/PhysRevB.89.035124 PACS number(s): 42.70.Qs, 42.25.Fx, 42.79.Fm

I. INTRODUCTION

The Bragg diffraction of waves gives rise to the appearance of band gaps in the energy spectra of various periodic structures. Representatives of these are photonic crystals (PhCs) [1–3], which have their band gaps in the electromagnetic spectrum, with the gap energy position governed by the period of the spatial modulation of the dielectric constant.

In 1995, a research team from Ioffe Physical-Technical Institute published a paper [4] that demonstrated that synthetic opals are in fact three-dimensional PhCs. This work has formed a basis for a series of technological, structural, and optical studies made in recent years [5–27].

Opals possess band gaps in the visible range due to the typical size of the constitutive a-SiO_2 particles of some hundreds of nanometers. This provides a unique chance to study photonic properties not only by traditional methods like registering transmission or reflection with a spectrometer, but also by directly observing diffraction patterns on a screen disposed behind or around the sample.

In the Bragg diffraction of light, the processes associated with the surface of the Brillouin zone (BZ) where the photonic stop bands open up are essential. The Bragg diffraction occurs when the Laue conditions are satisfied: $\mathbf{k}_s = \mathbf{k}_i + \mathbf{g}_{hkl}$, where $\mathbf{k}_i$ and $\mathbf{k}_s$ are the wave vectors of the incident and scattered light waves, respectively, and $\mathbf{g}_{hkl}$ is the reciprocal lattice vector determined by a system of scattering planes with Miller indices (hkl) (in the notation of the fcc lattice of opal). Earlier, the Bragg diffraction was studied both experimentally and theoretically in bulk samples of synthetic opals [4,10–13,17,18,20,23,25,26], thin opal films [5,8,14,15,19,21,24], and in colloidal opal-based PhCs [28,29]. These works were devoted to the study of specular reflection spectra and diffraction patterns [13,15,28,30–32], which were observed on screens, photographed, and processed using various programs.

If the Laue condition holds simultaneously for two systems of planes with different Miller indices ($h_1k_1l_1$) and ($h_2k_2l_2$), the optical spectra exhibit special effects caused by multiple Bragg diffraction (MBD) of light. The MBD was first revealed in x-ray scattering spectra of germanium crystals [33]. In PhCs, this phenomenon was first observed in optical studies of the high-contrast TiO_2 opal-based inverted structure [34]. A doublet structure was observed in specular reflection spectra, which was explained as a result of the simultaneous Bragg diffraction from the (111) and (200) planes in the region of the U point of the BZ of the fcc lattice. Here, the vector of the incident wave vector $\mathbf{k}_i$ scans the cross section $\Gamma L_g U_g X$ of the fcc BZ. Near the U_g point, the measured (111) and (200) dispersion curves deviate from the curves calculated using the Bragg equation and resemble the well-known effect of anticrossing of eigenstates of two interacting modes.

Subsequently, the MBD in different opal-based PhC was studied in a number of works. In Ref. [9], the unpolarized reflection spectra of films formed from polymethylmethacrylate spheres are presented. In these spectra, the authors observed a doublet structure, which, as in Ref. [34], was assigned to the MBD in the region of the U point of the BZ. The experimental data were compared with the results of calculations of photonic dispersion curves along the directions $L \rightarrow U$ and $X \rightarrow U$. In the region of the MBD, a doublet structure of the unpolarized reflection spectra was also observed in the study of films prepared from polystyrene spheres [35]. The MBD involving the (111) and ($\bar{1}$11) photonic stop bands was observed in the region of the K point of the BZ in studies of the polarized transmission spectra of synthetic opals a-SiO_2 [36]. The MBD was investigated in the polarized transmission and reflection spectra of a-SiO_2 films [37]; however, calculations of the band structure of opals, as in Ref. [36], were not performed. The MBD and the relation between the shape of reflection spectra and the character of deformation of quasispherical particles forming opal-based structures have been analyzed theoretically and the reflection spectra of these structures, including the region of the MBD, have been studied experimentally [38–42].

Note that to our best knowledge; there are no published experimental papers totally covering the MBD phenomenon in opal-based PhCs. The complete set of the experimental

*m.rybin@mail.ioffe.ru

data should include *two reflection spectra from* $(h_1k_1l_1)$ *and* $(h_2k_2l_2)$ *planes* together with transmission spectra. However, *in the previous works, the authors were limiting themselves only to the study of the reflection spot from a single set of planes*, generally (111) plane. The data on reflection from the $\{\bar{1}11\}$ and {200} planes have not been published. The problem is that the total internal reflection on the opal-air interface limits the range of angles accessible to the measurement. The light rays within the opal sample that strike the interface with the air (or any lower-index medium) at too large angle are totally reflected, and remain confined to the sample.

Here, our aim was to study the MBD from opal films using original experimental setup with a holder formed from two quartz semispheres. As a result, we overcome the problem of the total internal reflection in an opal film or in a substrate; so that the angle-resolved and frequency-resolved diffraction patterns demonstrating *two reflection spots* have been successfully investigated in various scattering geometries. The transmission spectra and diffraction patterns obtained did show pronounced effects causing by the MBD.

II. SAMPLE CHARACTERIZATION AND EXPERIMENTAL METHODS

Our experimental study dealt with opal films that were made up of spherical a-SiO_2 particles. The a-SiO_2 particles were produced by slow base hydrolysis of tetraethoxysilane in a water-alcohol medium [43]. A series of ordered films were grown by vertical deposition on a fused quartz substrate. Most of the experimental data presented below were obtained from an opal film, in which two sides of about 15×20 mm^2 formed a plane coinciding with the (111) crystallographic plane and the film has 24 layers of a-SiO_2 particles in thickness.

The goal of the present work was to investigate the MBD that takes place at the certain regions of the incident wave vector $\mathbf{k}_i$ and wave length λ. These regions can be defined from a photonic band structure. In this section, by photonic band structure we mean a set of (hkl) photonic dispersion curves calculated for special cross sections of the BZ and expressed in the "energy versus wave vector $\mathbf{k}$" coordinates or, what is equivalent, in the "Bragg wavelength λ_{hkl} versus propagation angle θ" coordinates (see Fig. 1). The calculations were performed using the following formula [3,17,18,23]:

$$\lambda_{hkl} = 2d_{111}n_{\text{opal}}\left(\frac{3}{h^2+k^2+l^2}\right)^{1/2}|\cos(\theta_{hkl})|, \qquad (1)$$

where d_{111} is the distance between the adjacent planes (111), $d_{111} = \sqrt{2/3}D = 296$ nm ($D = 350$ nm is the diameter of the a-SiO_2 spheres), $n_{\text{opal}} = 1.32$ is the average dielectric constant of the opal-filler fcc structure with air as a filler, and θ_{hkl} is the angle between the incidence wave vector $\mathbf{k}_i$ and reciprocal lattice vector $\mathbf{g}_{hkl}$. The calculations were performed for the high symmetry cross-section of the fcc BZ $\Gamma X L_g L$ and the results are presented in Fig. 1. For this scanning, the direction of the wave vector $\mathbf{k}_i$ is specified by the angle $\theta^{\text{opal}} = \theta_{111}$. We will denote the [111] direction as $\Gamma \rightarrow L_g$, in contrast to the three other equivalent directions $\Gamma \rightarrow L$ in an fcc lattice. Besides, the high-symmetry points on the BZ surface that belong to the same hexagonal plane as the L_g point will also be marked with the subscript g.

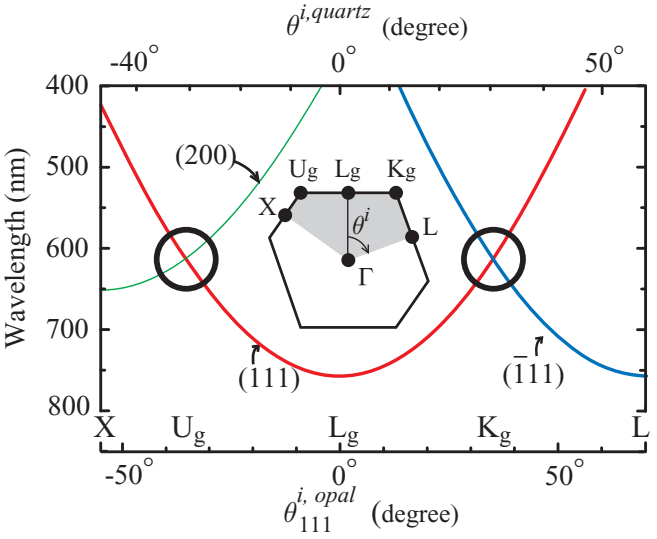

FIG. 1. (Color online) Low-energy photonic band structure of opal-based PhCs. The dependencies $\lambda_{hkl}\left(\theta^{\text{opal}}\right)$ are calculated from Eq. (1). The symmetry points of the surface of the first BZ are shown in the lower abscissa. The corresponding angles of light incidence θ from the quartz hemisphere onto an opal film calculated from Snell's law are shown in the upper abscissa. The points of the MBD are marked by cycles. (Insert) Cross-section of the BZ of the fcc lattice made by the scanning plane $\Gamma X L_g L$.

The MBD occurs on the surface of the first BZ at the points of the intersection of the dispersion curves, which are marked by circles in Fig. 1. The MBD takes place at the K_g point, owing to the intersection of the (111) and $(\bar{1}11)$ dispersion curves, while at the U_g point, owing to the intersection of the (111) and (200) dispersion curves. Note that the intensity of the (200) band in the optical spectra of opal samples with air as a filler is small (see Appendix). Therefore, in this paper, the MBD was investigated for the case of the intersection of the (111) and $(\bar{1}11)$ dispersion curves, which is observed at $\theta^{\text{opal}} = 35°$ (see Fig. 1).

We should emphasize the key feature of our experimental studies, namely, a technique of recording the diffraction patterns and transmission spectra. To overcome the restrictions caused by total internal reflection in a sample or in a substrate, thin opal film was placed at the center of a quartz holder consisting from two quartz hemispheres as shown in Fig. 2. The quartz refractive index $n_{\text{quartz}} = 1.45$ is relatively close to the refractive index of opal with air as a filler $n_{\text{opal-air}} = 1.32$ (e.g., Ref. [23]). As a result, most of the effects caused by the confinement of the diffracted light to the opal film or to the quartz film substrate were eliminated, which allowed making quantitative measurements of the spectral and angular dependencies of the diffracted light intensities. The diffraction spectra were measured in the regions of the specular reflection from the (111) and $(\bar{1}11)$ sets of planes that hereafter referred to as (111) and $(\bar{1}11)$ scattering geometries (see Fig. 2). The directions of the diffraction spots are defined by the kinematic relation $\mathbf{k}^s = \mathbf{k}^i + \mathbf{g}_{hkl}$ with $|\mathbf{k}^s| = |\mathbf{k}^i|$. The correspondence between in-holder angles θ and in-film angles θ^{opal} at the quartz-opal interface are defined by Snell's law.

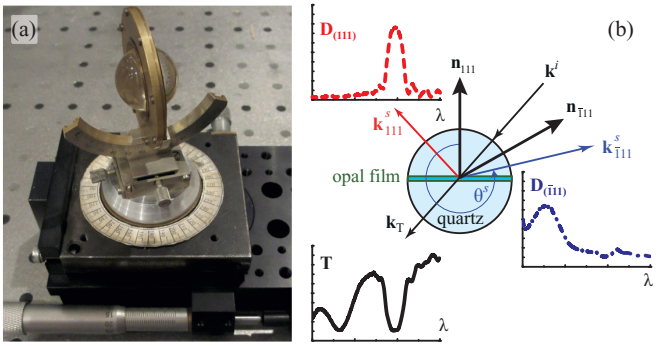

FIG. 2. (Color online) (a) The sample holder consisting from two quartz hemispheres with thin opal film in between. (b) The scheme shows the relation between $\mathbf{k}^i$ (the incident wave vector) and $\mathbf{k}_T$, $\mathbf{k}^s_{111}$, and $\mathbf{k}^s_{\bar{1}11}$ (the wave vectors of transmitted and diffracted light) and correspondent transmission T and diffraction D_{111}, $D_{\bar{1}11}$ spectra. The normal vectors $\mathbf{n}_{111}$, $\mathbf{n}_{\bar{1}11}$ to the (111), ($\bar{1}$11) sets of planes denote the [111] and [$\bar{1}$11] directions.

We investigated the behavior of the reflection spots and transmission spectra at varying the wave vector $\mathbf{k}^i$ orientation relative to the fcc opal lattice. The angular accuracy of the sample orientation was about 0.5°. An HL-2000 (Ocean Optics) halogen lamp was used as a white light source. The transmission spectra and reflection spots registered in the large solid angle were finally recorded by an Acton SP2500 spectrometer (Princeton Instruments) with a PIXIS-256 camera.

III. EXPERIMENTAL RESULTS: DIFFRACTION FROM THE ($\bar{1}$11) PLANES

In order to investigate the MBD in opal films, we performed a thorough investigation of the diffraction patters and transmission spectra. As we previously mentioned, the (111) diffraction reflex D_{111} was investigated in a number of experimental works [13,15,28,30–32,39]. Therefore our major task in making the experiments was to find and investigate the ($\bar{1}$11) diffraction reflex $D_{\bar{1}11}$. In this section, we will concentrate on its spectral and spatial properties.

In the diffraction experiments, the incident beam of white light scans the (01$\bar{1}$) plane of the fcc opal lattice that is perpendicular to both (111) and ($\bar{1}$11) planes (the wave vector $\mathbf{k}^i$ scans the $\Gamma L_g K_g L$ cross-section of the BZ). In such scattering geometry the beam reflected from (111) and ($\bar{1}$11) planes should also lie and be detectable in the (01$\bar{1}$) plane. The $D_{\bar{1}11}$ spectra were measured in the region of the specular reflection from the ($\bar{1}$11) set of planes (see Fig. 3), that is, in the ($\bar{1}$11) scattering geometry (see Fig. 2). The $D_{\bar{1}11}$ reflex was observed as a broad iridescent strip and its spectral structure was analyzed in detail as a function of the registration angle θ^s. Figure 4 illustrates the method we used for the acquisition of the ($\bar{1}$11) reflexes. For each incident angle θ, the angle-resolved reflectivity spectra $D_{(\bar{1}11)}$ were measured at various registration angles θ^s with a 2° step. Thereafter, the spectra were added up to obtain a final integral spectrum $D_{\bar{1}11}$. Figure 3 shows the angle- and frequency-resolved diffraction data taken in the ($\bar{1}$11) scattering geometry. We will present detailed discussion of these spectra together with transmission data in the next

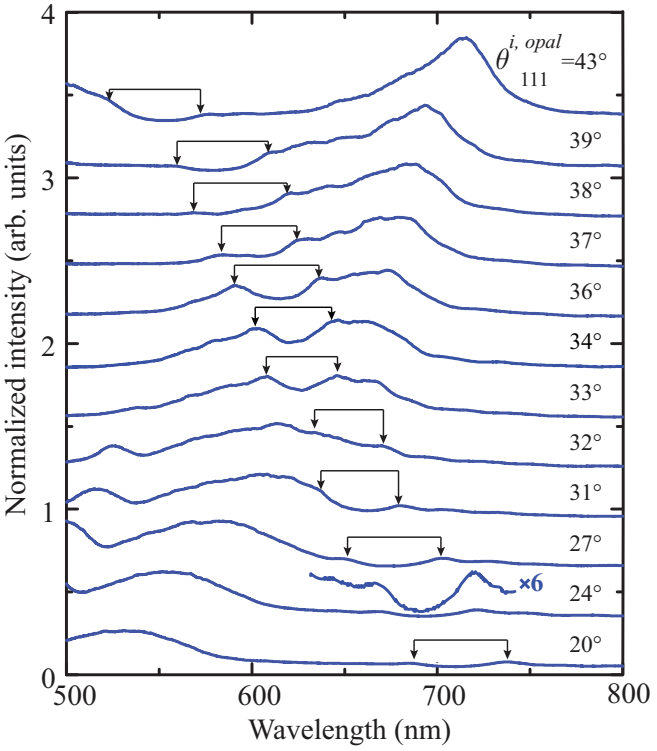

FIG. 3. (Color online) The integral spectra $D_{(\bar{1}11)}$ of the white light diffracted from the ($\bar{1}$11) planes of an opal film as a function of the incident angle θ^{opal}. The spectra obtained in the $\Gamma L_g K_g L$ scan of the fcc BZ. The thickness of the film is 24 layers of a-SiO_2 particles with the diameter $D = 350$ nm. The opal filler is air. The curves are shifted vertically by the constant value of 0.3. The cursors show "twin peaks", i.e., the traces of the (111) diffraction band. The insert (×6) shows the twin peaks in the enlarged scale.

section. Here, we point out several important characteristic features of the obtained spectra.

First, the comparison of the data given in Fig. 3 and the dispersion dependencies calculated from Eq. (1) (see Fig. 1) enable one to attribute unambiguously the $D_{\bar{1}11}$ reflex to the ($\bar{1}$11) photonic stop band. The experimental dependencies of the ($\bar{1}$11) band positions obtained from the spectra will be presented below in Sec. IV. Note that in all previous papers, the ($\bar{1}$11) reflex was observed only in the (111) scattering geometry in the region of the MBD when it crosses the (111) reflex.

Another interesting feature we found here is the trace of the (111) diffraction band in the $D_{(\bar{1}11)}$ spectra (see Fig. 3). For the 24-layer-thick film, the (111) band manifests itself as two small peaks ("twin peaks") and a dint of the stop band in between. To explain these features, we refer to dependencies of the group index n_g obtained for opal-based PhC [3,44]. Near the edges of the stop band, photonic dispersion curves deviate from linear behavior and become flat. Thus the group velocity exhibits pronounced slowing down at the band edge (spectral regions of slow light) and superluminal behavior (i.e., $v_g > c$) within the photonic stop band. The group index is the inverse group velocity normalized to the speed of light in vacuum $n_g = c/v_g$. According to the experimental and theoretical dependences, as the thickness of an opal film increases from ten layers, twin

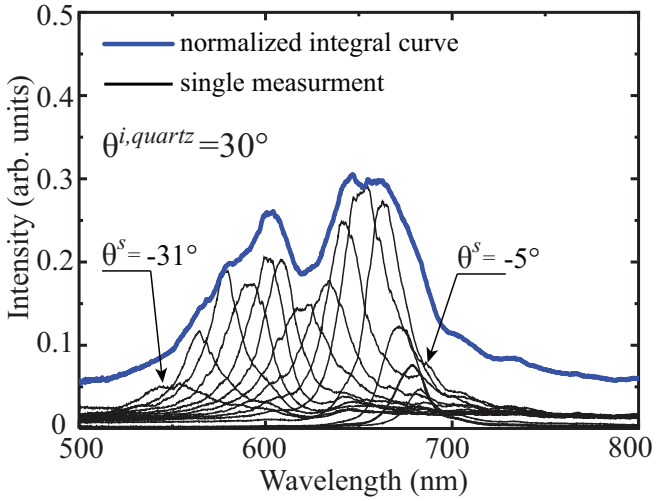

FIG. 4. (Color online) Diffraction spectra $D_{\bar{1}11}$ of an opal film registered at various scattering angles θ^s in the region of the MBD for white light incident angle $\theta^{i,\text{opal}} = 34^\circ$ (thin black curves). The thick blue curve represents the normalized integral spectra. The film has 24 layers of a-SiO_2 particles with the diameter $D = 350$ nm and the filler is air.

peaks of n_g develop at frequencies close to the stop band edges, and a region of low n_g appears in between [44]. This is exactly the behavior we can see in Fig. 3.

Another reason for the appearance of the twin peaks near the band edges is the disorder of real opal samples [25,26,45,46]. The microstructure of the a-SiO_2 particles leads to inhomogeneity of dielectric permittivity of a single particle and to dissimilarities in size and permittivity of a-SiO_2 particles in ensemble forming an opal sample [3,23,25]. In a pioneering work on light scattering in disordered PhC, S. John predicted that localization of light may occur in the vicinity of stop band edges [47]. Such interplay between Bragg diffraction and disorder-induced scattering was considered as a way to localize light and as a mechanism capable to suppress transmittance and increase back-scattering.

Therefore we would expect that the twin peaks structure in the $D_{\bar{1}11}$ spectra is a result of the increasing of the back-scattering due to microstructure of the a-SiO_2 particles or/and due to the bending of the dispersion curves at the stop band edges.

To investigate the spectral and spatial dispersion of the $(\bar{1}11)$ spot at the MBD condition, we carried out experiments on diffraction of white light with incidence angle $\theta^{\text{opal}} = 34^\circ$. The structure of the $(\bar{1}11)$ reflex was analyzed in detail as a function of the registration angle θ^s (Fig. 4). The measurements were made with a 2° step in the region of the $(\bar{1}11)$ reflected beam. As a result, strong spectral and spatial variation of the diffracted white light has been revealed. The iridescent $(\bar{1}11)$ spot is characterized by inhomogeneous broadening, the spectral line width of the integral band is about 120 nm and the angular width is about 20°. For each given registration angle $-31^\circ < \theta^s < -5^\circ$, the width of more homogeneous line is much smaller (about 20 to 30 nm).

Note that the integral spectral width of both (111) and $(\bar{1}11)$ spots out of the MBD region is about 50 nm. This value is equal to the spectral width that was obtained for (111) spot in diffraction experiments on bulk opal samples [13,30]. It means that the opal film under study has rather perfect structure with highly ordered nongrowth $(\bar{1}11)$ layers.

IV. COMPARISION OF DIFFRACTION AND TRANSMISSION EXPERIMENTAL DATA

In this section, we present a unique collection of the spatial—and frequency—resolved optical responses of an opal film to the white light excitation. Figure 5 shows the data of the diffraction (D_{111} and $D_{\bar{1}11}$) and transmission (T) experiments obtained on the 24 layer thick opal film in the $\Gamma L_g K_g L$ scan of the fcc BZ as a function of the incidence angle θ^{opal}. To discuss

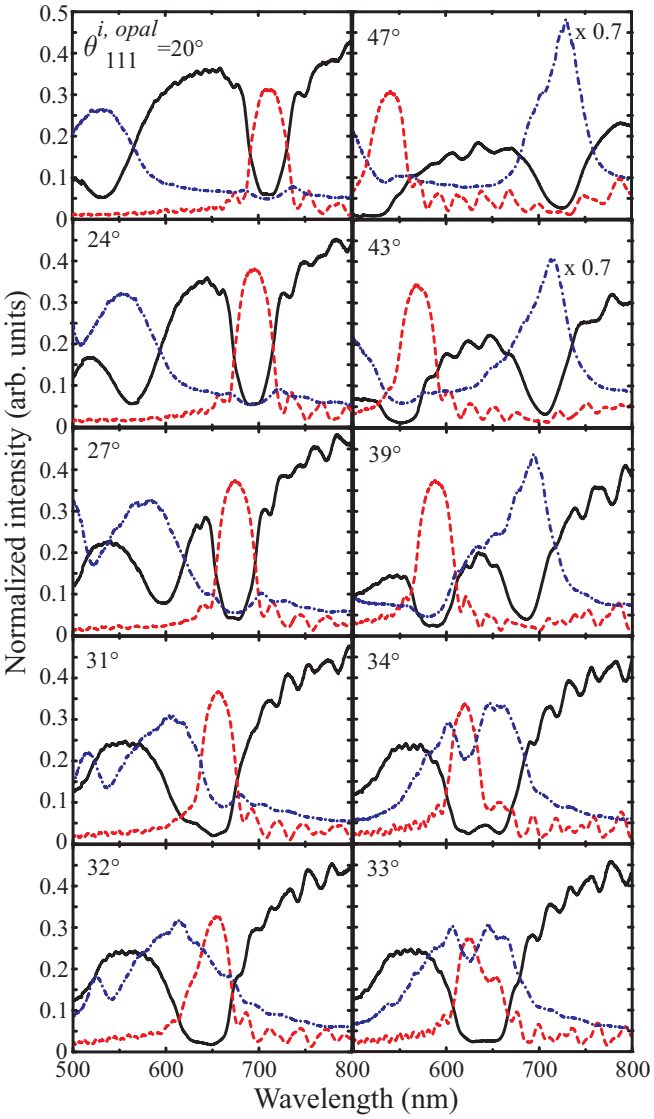

FIG. 5. (Color online) The angle-resolved optical spectra of the 24 layer thick opal film with air as a filler (a-SiO_2 particles diameter $D = 350$ nm). The spectra obtained in the $\Gamma L_g K_g L$ scan of the fcc BZ as a function of the angle θ^{opal} in the region of the MBD. The black solid curves show transmission (T) spectra; the red dashed curves show D_{111} diffraction spectra; the blue dot-and-dashed curves show $D_{\bar{1}11}$ diffraction spectra.

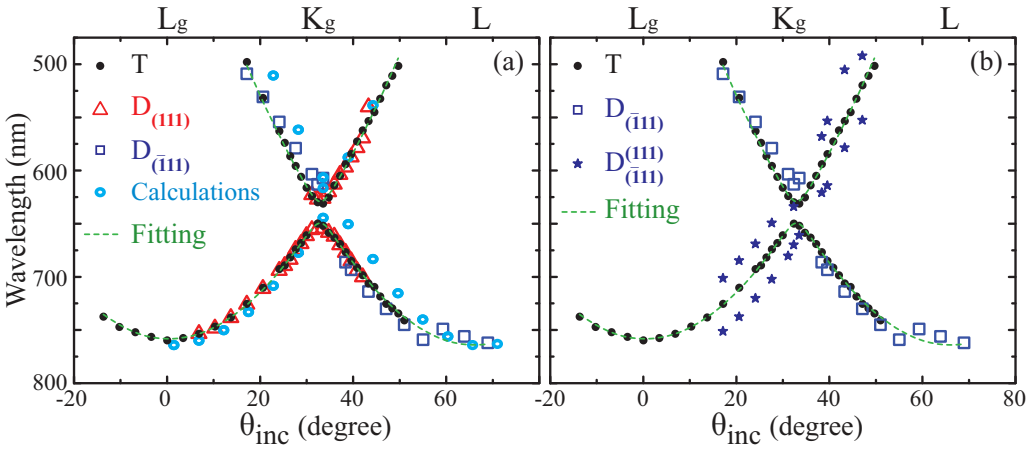

FIG. 6. (Color online) Experimental and calculated spectral positions of (111) and ($\bar{1}11$) bands in the transmission and reflection spectra and of the twin peaks structure in the $D_{(\bar{1}11)}$ spectra. The sample is the 24-layer-thick opal film with air as a filler (a-SiO_2 particles diameter $D = 350$ nm). The green dash lines represent best fits to the data using the phenomenological approach described in Ref. [38]. The black circles show the data obtained from transmission (T) spectra; the red triangles are related to the data obtained from $D_{(111)}$ diffraction spectra; the blue squares indicate the data obtained from $D_{(\bar{1}11)}$ diffraction spectra; the blue stars point out the traces of the (111) diffraction band in $D_{(\bar{1}11)}$ diffraction spectra; the cyan symbols denote position of the peaks in calculated reflection spectra.

the MBD effects, we will compare the transmission and reflection spectra to each other. The measurements were made with a 2° step that allows us to analyze the dependences with particular thoroughness. Figure 5 demonstrates general agreement between two dips in the transmission spectrum and the two diffraction peaks (111) and ($\bar{1}11$) for each incident angle θ^{opal}.

The D_{111} diffraction spectra were collected in the (111) scattering geometry (see Fig. 2). For incident angles θ^{opal} far from the MBD region, the D_{111} diffraction spectra contain single strong reflection from (111) band. Fabry-Pérot oscillations originating from the finite thickness of the opal film are superimposed over the background (see Fig. 5). As we already mentioned, the diffraction spectrum $D_{\bar{1}11}$ contains a pronounced background superimposed by three bands: strong ($\bar{1}11$) diffraction band and twin peaks.

As to the transmission spectrum, far from the MBD region, it consists from two strong (111) and ($\bar{1}11$) bands. Note that the dissimilarity in permittivity of a-SiO_2 particles caused the background that can be described as Mie scattering with more intense forward lobe [3]. The interference between Bragg diffraction and disorder-induced Mie scattering leads to a Fano resonance [25,26,48] and a transmission spectrum exhibiting a Bragg dip with an asymmetric profile. In opals, the Fano asymmetry parameter q is linked with the dielectric contrast between the permittivity of the filler ($\varepsilon_{\text{filler}} = 1$ in our case) and the specific value determined by the opal matrix ($\varepsilon_f^0 = 1.82$)[25]. According to the experimental results [25,26] for $(\varepsilon_{\text{filler}} - \varepsilon_f^0) < 0$, the long-wavelength wing of the (111) stop band is relatively flat in contrast to a steep short-wavelength wing. This is the asymmetric profile that we can observe in Fig. 5. Note that in the reflectance we can not observe any asymmetry of the (111) peak due to absence of the strong background that is necessary for the Fano interference.

Let us compare the experimental transmission and diffraction spectra for selected incidence angles θ^{opal} that demonstrate the most specific features of the MBD at the K_g point of the BZ due to intersection of the (111) and ($\bar{1}11$) dispersion curves (see Fig. 1). The experimental dependencies of the band positions obtained from the spectral treatment are presented in Fig. 6. Outside the MBD region, the dispersion of the (111) and ($\bar{1}11$) photonic bands is well described by Eq. (1), i.e., it corresponds to the Bragg condition. In the MBD region (the K_g point of the BZ), the anticrossing effect is observed both in transmission and in reflection: the (111) and ($\bar{1}11$) bands do not intersect and the spectra have a doublet structure (see Fig. 6). When the (111) and ($\bar{1}11$) bands are separated by the closest distance ($\theta^{\text{opal}} = 32°$ to 33°, Fig. 5), one can see a doublet structure with a weak dip and a total line full width at half maximum (FWHM) $\Delta\lambda \approx 70$ nm, which is nearly two times larger than FWHM of one (111) or ($\bar{1}11$) band ($\Delta\lambda \approx 40$ nm) outside the MBD region.

Note that in addition to the previous results on the MBD in opal-like PhC [9,34,35,37,38,40–42], here we present the ($\bar{1}11$) dispersion dependence extracted from the diffraction data and the twin peak structure that has direct relationship with the (111) band (see Fig. 6). It was possible to find the twin peak structure owing to the pronounced background in the ($\bar{1}11$) scattering geometry. Such structure was never observed before because the background intensity in the well-studied (111) scattering geometry is very weak (see Fig. 5).

V. CONCLUSIONS

In this work, the MBD in synthetic opals has been investigated using a complex approach that combines an experimental study of transmission and diffraction spectra with theoretical calculations of the photonic band structure. Due to the experimental setup, we registered with a high angular resolution the intensity of light scattered into the large solid angle of the back hemisphere, which allowed to make quantitative measurements of the spectral and spatial dependencies of the (111) and ($\bar{1}11$) diffraction reflexes. The setup allowed us (i) to distinguish the ($\bar{1}11$) diffraction patterns and (ii) to find twin-peak structure in the ($\bar{1}11$)

spectrum originating from the (111) diffraction band. The $(\bar{1}11)$ diffraction reflex we succeed to observe through all investigated angular region.

An essential spectral feature of opal-based PhCs is a constructive or destructive interference of different diffracted waves. We have observed and discussed two opposite cases of such interference. The first one is the MBD caused by the interference of two spectrally narrow Bragg bands (111) and $(\bar{1}11)$. When the incident wave vector $\mathbf{k}^i$ scans the cross section $\Gamma L_g K_g L$ of the fcc BZ and approaches the K_g point, the (111) and $(\bar{1}11)$ dispersion curves should intersect. In reality, due to interference of waves, a doublet structure is observed through all investigated angular region, the dispersion curves deviate from those calculated using the Bragg equation and demonstrate the anticrossing regime characteristic for two interacting modes. The second case is the interference of the (111) Bragg band and disorder-induced broad Mie scattering. The interference of a narrow band with a broad background gives rise to a Fano resonance that manifests itself in a characteristically asymmetric line shape of the Bragg band in transmission spectra.

ACKNOWLEDGMENTS

We are grateful to A. A. Kaplyanskii and N. V. Nikonorov for support and critical comments and to A. V. Moroz for experimental assistance and useful discussions. This work was financially supported by Government of Russian Federation, Grant 074-U01.

APPENDIX: PHOTONIC BAND STRUCTURE CALCULATIONS

We consider the sample as a layer of width d cut from infinite PhC. Let x and y axes define the orientation of the layer boundaries and z axis to be normal to the layer surfaces. An electromagnetic field inside the layer can be constructed as a sum of solutions to the Maxwell's equations of infinite PhC. As is well known, the propagating modes in a periodic system form a band structure [1] and the evanescent solutions with imaginary wave vectors usually are not taken into consideration because they demonstrate exponential growth in a certain direction. However, in the case of a structure with a boundary, we have to take into account evanescent solutions as well as propagating modes because in this case exponential growth is limited by the boundary. Our interest is in the electromagnetic field excited by the incident wave, say it is an s-polarized wave with $k_z > 0, k_y = 0$, and $E_x = E_z = 0$. The boundary conditions require conservation of wave vector's x component. So we have two problems: (i) to calculate the solutions to the Maxwell equations with fixed k_x and (ii) to find the amplitudes of these solutions and the amplitudes of scattered waves that would satisfy the boundary conditions.

1. General approach

The standard approaches to the calculation of the band structure, i.e., dispersion relations $\omega(\mathbf{k})$, are based on finding the frequency ω for a given wave vector $\mathbf{k}$ [1,49–51]. However, in our case, those approaches are not applicable. We consider the inverse dispersion problem of finding solutions with a given frequency and with fixed two components of the wave vector. We start from the pair of Maxwell's equations with curls for the spatially dependent parts of the magnetic $\mathbf{H}$ and electric $\mathbf{E}$ fields in a matrix form:

$$\nabla_\times \begin{pmatrix} \mathbf{E} \\ \mathbf{H} \end{pmatrix} = -\omega \begin{pmatrix} 0 & -i \\ i & 0 \end{pmatrix} \begin{pmatrix} \varepsilon_0 \varepsilon & 0 \\ 0 & \mu_0 \mu \end{pmatrix} \begin{pmatrix} \mathbf{E} \\ \mathbf{H} \end{pmatrix}, \tag{A1}$$

Here, $\nabla_\times$ is a curl operator, and it is assumed to give an $\exp(-i\omega t)$ factor at all fields.

In the case of periodical structure, a field $\mathbf{X}$ can be written as Bloch waves $\mathbf{X} = e^{i\mathbf{kr}}\mathbf{x}(\mathbf{r})$, where $\mathbf{x}(\mathbf{r})$ is a periodic function that possesses translation symmetry of the lattice ($\mathbf{X}$ can be either $\mathbf{E}$ or $\mathbf{H}$). By substitution of the fields in a Bloch wave form to Eq. (A1) and by separation of the tangential part of the wave vector $\mathbf{k}_\tau$ and normal component k_z, we get a generalized eigenproblem for the unknown eigenvalue k_z and fields $(\mathbf{e},\mathbf{h})^T$:

$$\left[i\left(\nabla_\times + i\mathbf{k}_\tau \times\right) + \omega \begin{pmatrix} 0 & \mu_0\mu \\ -\varepsilon_0\varepsilon & 0 \end{pmatrix} \right] \begin{pmatrix} \mathbf{e} \\ \mathbf{h} \end{pmatrix} = k_z \mathbf{n}_z \times \begin{pmatrix} \mathbf{e} \\ \mathbf{h} \end{pmatrix}. \tag{A2}$$

Here, cross-product acts on vectors $\mathbf{e}$ and $\mathbf{h}$.

The cross-product $\mathbf{n}_z\times$ is related to the matrix of rank 2. As a result, there are solutions with infinite k_z, which are prohibited by the pair of the Maxwell's equations with divergence. However, we can exclude these two solutions by the straightforward procedure of e_z and h_z elimination. After that, the generalized eigenproblem (A2) reduces to the eigenproblem for k_z and tangential components of fields $\mathbf{e}$ and $\mathbf{h}$.

2. Plane-wave expansion

The periodic functions $\mathbf{e}$ and $\mathbf{h}$ can be expanded in the Fourier series $\sum_{\mathbf{g}} \mathbf{x}_\mathbf{g} \exp(i\mathbf{gr})$. We consider only few reciprocal lattice vectors, since the expansion coefficients $\mathbf{x}_\mathbf{g}$ are negligible when the product $\mathbf{kg}$ is far from $|\mathbf{g}|/2$, (i.e., not under the Bragg condition) [3]. If all of the reciprocal lattice vectors have no y components, the eigenproblem can be splitted for two polarizations. For s and p polarizations, they read

$$\begin{pmatrix} i\frac{\partial}{\partial z} & -\omega\mu_0 \\ -\omega\varepsilon_0\varepsilon + \frac{1}{\omega\mu_0}\hat{\kappa}^2 & i\frac{\partial}{\partial z} \end{pmatrix} \begin{pmatrix} e_y \\ h_x \end{pmatrix} = k_z \begin{pmatrix} e_y \\ h_x \end{pmatrix} \tag{A3}$$

and

$$\begin{pmatrix} i\frac{\partial}{\partial z} & \omega\mu_0 - \hat{\kappa}\frac{1}{\omega\varepsilon_0\varepsilon}\hat{\kappa} \\ \omega\varepsilon_0\varepsilon & i\frac{\partial}{\partial z} \end{pmatrix} \begin{pmatrix} e_x \\ h_y \end{pmatrix} = k_z \begin{pmatrix} e_x \\ h_y \end{pmatrix}, \tag{A4}$$

respectively. Here, we introduced an operator $\hat{\kappa} = (i\frac{\partial}{\partial x} - k_x)$.

Next, we are focused on the case of s polarization. The eigenvalue problem for fields in the plane-wave representation is as follows:

$$[\hat{M}_0 - \hat{V}] \begin{pmatrix} e_\mathbf{g} \\ h_\mathbf{g} \end{pmatrix} = k_z \begin{pmatrix} e_\mathbf{g} \\ h_\mathbf{g} \end{pmatrix}, \tag{A5}$$

where the unperturbed operator that is related to the so-called empty lattice approximation is

$$\hat{M}_0 = -g_z + \frac{(g_x + k_x)^2}{\omega\mu_0} \begin{pmatrix} 0 & 0 \\ 1 & 0 \end{pmatrix} - \omega \begin{pmatrix} 0 & \mu_0 \\ \varepsilon_0\tilde{\varepsilon}_0 & 0 \end{pmatrix} \tag{A6}$$

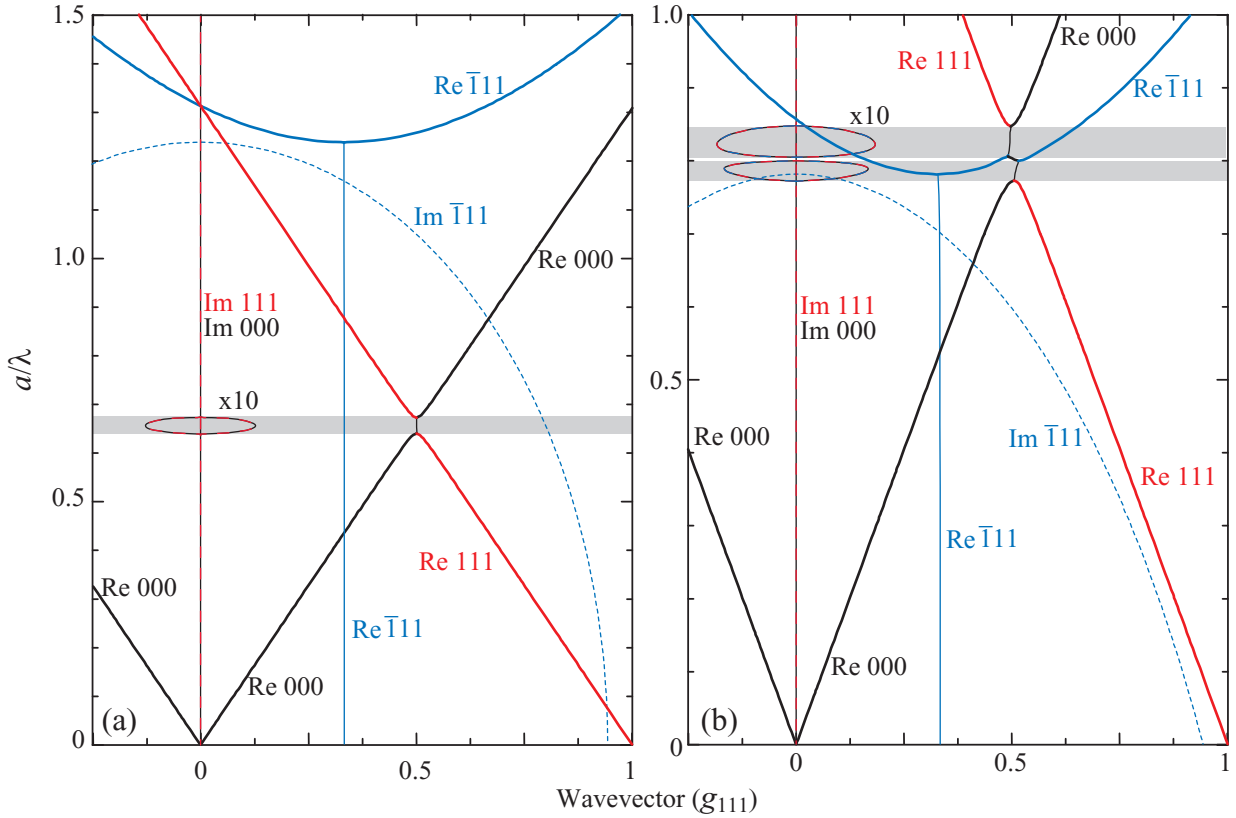

FIG. 7. (Color online) Photonic band structure with account of three reciprocal lattice vectors 0, $\mathbf{g}_{111}$, and $\mathbf{g}_{\bar{1}11}$. Thick lines represent solutions with real wave vectors. Thin and dashed lines represent real and imaginary parts of k_z for evanescent solutions. (a) Normal incident $k_x = 0$. (b) Multiple Bragg diffraction regime. Imaginary parts within photonic band gaps (shaded areas) are multiplied by ten. Dispersion bands are assigned to (hkl) reciprocal lattice vectors: black curve for (000), red curve for (111), and blue curve for $(\bar{1}11)$. Curves for the real and imaginary parts of wave vector are signed by Re and Im, respectively.

and operator that mixes different bands reads

$$\hat{V} = \omega \sum_{\mathbf{g}' \neq \mathbf{g}} \begin{pmatrix} 0 & 0 \\ \varepsilon_0 \tilde{\varepsilon}_{\mathbf{g}-\mathbf{g}'} & 0 \end{pmatrix} \begin{pmatrix} e_{\mathbf{g}'} \\ h_{\mathbf{g}'} \end{pmatrix}. \tag{A7}$$

Here,

$$\tilde{\varepsilon}_{\mathbf{g}} = \frac{1}{V_{\text{cell}}} \iiint_{V_{\text{cell}}} \varepsilon(\mathbf{r}) \exp(-i\mathbf{gr})\, d\mathbf{r}. \tag{A8}$$

In the case of the fcc structure consisting of close-packed spherical scatterers, we have

$$\tilde{\varepsilon}_0 = \frac{\pi}{3\sqrt{2}} [\varepsilon_s - \varepsilon_b] + \varepsilon_b, \tag{A9}$$

and for $\mathbf{g}_{hkl} \neq 0$,

$$\tilde{\varepsilon}_{hkl} = \frac{2}{\pi^2 (h^2 + k^2 + l^2)^{3/2}} (\varepsilon_s - \varepsilon_b)(\sin x - x \cos x), \tag{A10}$$

where ε_s and ε_b are the sphere and surrounding material permittivities, $x = (\pi/\sqrt{2})\sqrt{h^2 + k^2 + l^2}$. The numerical values of the low indices $\tilde{\varepsilon}_{hkl}$ are the following: $\tilde{\varepsilon}_{111} = (\varepsilon_s - \varepsilon_b)\, 8.88 \times 10^{-2}$, $\tilde{\varepsilon}_{200} = (\varepsilon_s - \varepsilon_b)\, 5.55 \times 10^{-3}$, $\tilde{\varepsilon}_{220} = -(\varepsilon_s - \varepsilon_b)\, 5.63 \times 10^{-2}$, $\tilde{\varepsilon}_{311} = -(\varepsilon_s - \varepsilon_b)\, 1.42 \times 10^{-2}$, and $\tilde{\varepsilon}_{222} = -(\varepsilon_s - \varepsilon_b)\, 1.11 \times 10^{-3}$. It is enough to take into account the reciprocal lattice vectors 0, $\mathbf{g}_{111} = g(0,0,1)$, and $\mathbf{g}_{\bar{1}11} = (g/3)(\sqrt{8},0,1)$, where g is the modulus of the reciprocal lattice vector 111.

Calculated photonic band structures are demonstrated in Fig. 7. The eigenvalues of the problem (A6), i.e., in the empty lattice approximation, form hypercones with apices in the reciprocal lattice sites. Therefore the photonic band structure represents a cross-section of this cones by a plane defined by k_x (related to the incident angle). We have taken into account three reciprocal lattice vectors and as a result in Fig. 7 there are sections of the three hypercones assigned by hkl indices. We consider three pairs of the eigenvalues, we got one pair for each hypercone. The plane intersects two hypercones with apices at the origin and at $\mathbf{g}_{111}$ for any frequencies and does not intersect the one with the apex at $\mathbf{g}_{\bar{1}11}$ at low frequencies. However, the last hypercone can intersect the plane if we assume that k_z may have imaginary part (it increases with the decrease of the frequency). Another opportunity for the imaginary part to exist is hypercone intersections, which are defined by the band mixing operator (A7). These intersections are exhibited as band gaps that can be assigned to reciprocal lattice vector $\mathbf{g}_{hkl} = \mathbf{g} - \mathbf{g}'$. The width of the (hkl) band gap is related to the matrix element value $\omega\varepsilon_0\tilde{\varepsilon}_{hkl}$.

Now, let us consider the most interesting case of the intersections of three hypercones [see Fig. 7(b)]. The interference

of three bands results in the band with the real k_z to exist between two gaps for any angles of incidence. In this case, we can not assign band gaps to specific (hkl) indices because the band is formed by mixing of modes associated with the hypercone at the origin and two other ones.

3. Transmission and reflection coefficients

Now we can find the transmission and reflection coefficients. The field inside the layer may contain harmonics k_x as well as $k_x + g_x$ for each reciprocal lattice vector. We considered only three reciprocal vectors, 0, $\mathbf{g}_{111} = g(0,0,1)$, and $\mathbf{g}_{\bar{1}11} = (g/3)(\sqrt{8},0,1)$, and have only two tangential harmonics k_x and $k_x + g\sqrt{8/9}$. Hence boundary conditions give eight equations (two harmonics at each boundary for electric and magnetic fields). Also, there are eight unknowns: four scattering coefficients (the pair of harmonics at each side) and four solutions to the Maxwell's equations in the layer. Note that unique solutions are only the ones within the range $[\alpha;\alpha + g]$ for any α (for BZ $\alpha = -g/2$). In general, it is straightforward to show that if we consider n harmonics, there are $2n$ unique solutions that can be found.

For each harmonic $q = k_x + g_x$, the boundary condition for tangential electric and magnetic fields reads

$$\sum_i \left\{ b_i \sum_{g_x=q} e_{\mathbf{g},i} \exp\left[i(k_z + g_z)z_b\right] \right\} - s_q^{\pm} = 0, \qquad \text{(A11)}$$

$$\sum_i \left\{ b_i \sum_{g_x=q} h_{\mathbf{g},i} \exp\left[i(k_z + g_z)z_b\right] \right\} \pm \frac{s_q^{\pm}}{\omega\mu_0} q_z = 0. \qquad \text{(A12)}$$

Here, b_i is the amplitude of the solution to the Maxwell's equation inside the layer, $s_q^{\pm}$ is the amplitude of the plane wave scattered by the layer. The plus is related to the side from the negative z direction and the minus is related to the other side. The normal component of the wave vector of a plane wave outside the layer is $q_z = \sqrt{\frac{\omega^2}{c^2}\varepsilon\mu - (k_x + g_x)^2}$. Besides zero, the right-hand side for the two equations, for $q = k_x$, should be replaced by the amplitude of the incident wave, i.e., unity for the electric field and $q_z/(\omega\mu_0)$ for the magnetic field with the appropriate sign. We should note that if $q + k_z$ is big enough, total internal reflection may arise and the corresponding coefficient should vanish. The calculated spectra have been processed and the dips in the transmission and the peaks in the other coefficients are in good agreement with the experiment [see Fig. 6(a)].

[1] J. D. Joannopoulos, S. G. Johnson, J. N. Winn, and R. D. Meade, *Photonic Crystals: Molding the Flow of Light*, 2nd ed. (Princeton University Press, Princeton, NJ, 2008).

[2] K. Sakoda, *Optical Properties of Photonic Crystals*, 2nd. ed. (Springer, Berlin, 2004).

[3] *Optical Properties of Photonic Structures: Interplay of Order and Disorder*, edited by M. F. Limonov and R. M. De La Rue (CRC Press, Taylor & Francis Group, 2012).

[4] V. N. Astratov, V. N. Bogomolov, A. A. Kaplyanskii, A. V. Prokofiev, L. A. Samoilovich, S. M. Samoilovich, and Y. A. Vlasov, Nuovo Cimento D **17**, 1349 (1995).

[5] H. Míguez, C. López, F. Meseguer, A. Blanco, L. Vázquez, R. Mayoral, M. Ocana, V. Fornés, and A. Mifsud, Appl. Phys. Lett. **71**, 1148 (1997).

[6] V. N. Bogomolov, V. G. Golubev, N. F. Kartenko, D. A. Kurdyukov, A. B. Pevtsov, A. V. Prokof'ev, V. V. Ratnikov, N. A. Feoktistov, and N. V. Sharenkova, Tech. Phys. Lett. **24**, 326 (1998).

[7] M. S. Thijssen, R. Sprik, J. E. G. J. Wijnhoven, M. Megens, T. Narayanan, A. Lagendijk, and W. L. Vos, Phys. Rev. Lett. **83**, 2730 (1999).

[8] J. F. Bertone, P. Jiang, K. S. Hwang, D. M. Mittleman, and V. L. Colvin, Phys. Rev. Lett. **83**, 300 (1999).

[9] S. G. Romanov, T. Maka, C. M. Sotomayor Torres, M. Müller, R. Zentel, D. Cassagne, J. Manzanares-Martinez, and C. Jouanin, Phys. Rev. E **63**, 056603 (2001).

[10] V. N. Astratov, A. M. Adawi, S. Fricker, M. S. Skolnick, D. M. Whittaker, and P. N. Pusey, Phys. Rev. B **66**, 165215 (2002).

[11] A. V. Baryshev, A. V. Ankudinov, A. A. Kaplyanskii, V. A. Kosobukin, M. F. Limonov, K. B. Samusev, and D. E. Usvyat, Phys. Solid State **44**, 1648 (2002).

[12] D. A. Mazurenko, R. Kerst, J. I. Dijkhuis, A. V. Akimov, V. G. Golubev, D. A. Kurdyukov, A. B. Pevtsov, and A. V. Sel'kin, Phys. Rev. Lett. **91**, 213903 (2003).

[13] A. V. Baryshev, A. A. Kaplyanskii, V. A. Kosobukin, M. F. Limonov, and A. P. Skvortsov, Phys. Solid State **46**, 1331 (2004).

[14] J. F. Galisteo-López, F. García-Santamaría, D. Golmayo, B. H. Juárez, C. López, and E. Palacios-Lidón, Photon. Nanostruct.: Fundam. Applic. **2**, 117 (2004).

[15] F. García-Santamaría, J. F. Galisteo-López, P. V. Braun, and C. López, Phys. Rev. B **71**, 195112 (2005).

[16] A. L. Pokrovsky, V. Kamaev, C. Y. Li, Z. V. Vardeny, A. L. Efros, D. A. Kurdyukov, and V. G. Golubev, Phys. Rev. B **71**, 165114 (2005).

[17] M. V. Rybin, K. B. Samusev, and M. F. Limonov, Photon. Nanostruct.: Fundam. Applic. **5**, 119 (2007).

[18] M. V. Rybin, K. B. Samusev, and M. F. Limonov, Phys. Solid State **49**, 2280 (2007).

[19] M. Ishii, M. Harada, A. Tsukigase, and H. Nakamura, J. Opt. A **9**, S372 (2007).

[20] A. V. Baryshev, A. B. Khanikaev, M. Inoue, P. B. Lim, A. V. Sel'kin, G. Yushin, and M. F. Limonov, Phys. Rev. Lett. **99**, 063906 (2007).

[21] I. Popa and F. Marlow, ChemPhysChem **9**, 1541 (2008).

[22] S. A. Grudinkin, S. F. Kaplan, N. F. Kartenko, D. A. Kurdyukov, and V. G. Golubev, J. Phys. Chem. C **112**, 17855 (2008).

[23] M. V. Rybin, A. V. Baryshev, A. B. Khanikaev, M. Inoue, K. B. Samusev, A. V. Sel'kin, G. Yushin, and M. F. Limonov, Phys. Rev. B **77**, 205106 (2008).

[24] G. Lozano, L. A. Dorado, D. Schinca, R. A. Depine, and H. Míguez, Langmuir **25**, 12860 (2009).

[25] M. V. Rybin, A. B. Khanikaev, M. Inoue, K. B. Samusev, M. J. Steel, G. Yushin, and M. F. Limonov, Phys. Rev. Lett. **103**, 023901 (2009).
[26] M. V. Rybin, A. B. Khanikaev, M. Inoue, A. K. Samusev, M. J. Steel, G. Yushin, and M. F. Limonov, Photon. Nanostruct.: Fundam. Applic. **8**, 86 (2010).
[27] G. Lozano, J. E. Mazzaferri, L. A. Dorado, S. Ledesma, R. A. Depine, and H. Míguez, J. Opt. Soc. Am. B **27**, 1394 (2010).
[28] R. M. Amos, J. G. Rarity, P. R. Tapster, T. J. Shepherd, and S. C. Kitson, Phys. Rev. E **61**, 2929 (2000).
[29] A. Tikhonov, R. D. Coalson, and S. A. Asher, Phys. Rev. B **77**, 235404 (2008).
[30] A. V. Baryshev, V. A. Kosobukin, K. B. Samusev, D. V. Usvyat, and M. F. Limonov, Phys. Rev. B **73**, 205118 (2006).
[31] M. V. Rybin, I. S. Sinev, A. K. Samusev, K. B. Samusev, E. Y. Trofimova, D. A. Kurdyukov, V. G. Golubev, and M. F. Limonov, Phys. Rev. B **87**, 125131 (2013).
[32] A. K. Samusev, K. B. Samusev, M. V. Rybin, M. F. Limonov, E. Y. Trofimova, D. A. Kurdyukov, and V. G. Golubev, Phys. Solid State **53**, 1056 (2011).
[33] M. Renninger, Z. Phys. **106**, 141 (1937).
[34] H. M. van Driel and W. L. Vos, Phys. Rev. B **62**, 9872 (2000).
[35] J. F. Galisteo-López, E. Palacios-Lidón, E. Castillo-Martínez, and C. López, Phys. Rev. B **68**, 115109 (2003).
[36] A. V. Baryshev, A. B. Khanikaev, H. Uchida, M. Inoue, and M. F. Limonov, Phys. Rev. B **73**, 033103 (2006).
[37] A. V. Baryshev, A. B. Khanikaev, R. Fujikawa, H. Uchida, and M. Inoue, Phys. Rev. B **76**, 014305 (2007).
[38] A. V. Moroz, M. F. Limonov, M. V. Rybin, and K. B. Samusev, Phys. Solid State **53**, 1105 (2011).
[39] G. M. Gajiev, V. G. Golubev, D. A. Kurdyukov, A. V. Medvedev, A. B. Pevtsov, A. V. Sel'kin, and V. V. Travnikov, Phys. Rev. B **72**, 205115 (2005).
[40] V. G. Fedotov and A. V. Sel'kin, Phys. Solid State **53**, 1140 (2011).
[41] S. Baek, A. V. Baryshev, and M. Inoue, Appl. Phys. Lett. **98**, 101111 (2011).
[42] A. Tikhonov, J. Bohn, and S. A. Asher, Phys. Rev. B **80**, 235125 (2009).
[43] E. Y. Trofimova, A. E. Aleksenskii, S. A. Grudinkin, I. V. Korkin, D. A. Kurdyukov, and V. G. Golubev, Colloid J. **73**, 546 (2011).
[44] J. F. Galisteo-López, M. Galli, M. Patrini, A. Balestreri, L. C. Andreani, and C. López, Phys. Rev. B **73**, 125103 (2006).
[45] R. Rengarajan, D. Mittleman, C. Rich, and V. Colvin, Phys. Rev. E **71**, 016615 (2005).
[46] E. Palacios-Lidón, B. H. Juárez, E. Castillo-Martínez, and C. López, J. Appl. Phys. **97**, 063502 (2005).
[47] S. John, Phys. Rev. Lett. **58**, 2486 (1987).
[48] A. N. Poddubny, M. V. Rybin, M. F. Limonov, and Y. S. Kivshar, Nat. Commun. **3**, 914 (2012).
[49] K. M. Ho, C. T. Chan, and C. M. Soukoulis, Phys. Rev. Lett. **65**, 3152 (1990).
[50] H. S. Sözüer, J. W. Haus, and R. Inguva, Phys. Rev. B **45**, 13962 (1992).
[51] S. G. Johnson and J. D. Joannopoulos, Opt. Express **8**, 173 (2001).